# Characterizing the spatiotemporal variations of evapotranspiration and aridity index in mid-western China from 2001 to 2016

MU Le, LU Yixiao, LIU Minguo, YANG Huimin*, FENG Qisheng*

State Key Laboratory of Grassland Agro-ecosystems, College of Pastoral Agriculture Science and Technology, Lanzhou University, Lanzhou 730020, China



**Abstract:** Mid-western China is one of the most sensitive and fragile areas on the Earth. Evapotranspiration (ET) is a key part of hydrological cycle in these areas and is affected by both global climate change and human activities. The dynamic changes in ET and potential evapotranspiration (PET), which can reflect water consumption and demand, are still unclear, and there is a lack of predictive capacity on drought severity. In this study, we used global MODIS (moderate-resolution imaging spectroradiometer) terrestrial ET (MOD16) products, Morlet wavelet analysis, and simple linear regression to investigate the spatiotemporal variations of ET, PET, reference ET ($ET_0$), and aridity index (AI) in mid-western pastoral regions of China (including Gansu Province, Qinghai Province, Ningxia Hui Autonomous Region, and part of Inner Mongolia Autonomous Region) from 2001 to 2016. The results showed that the overall ET gradually increased from east to southwest in the study area. Actual ET showed an increasing trend, whereas PET tended to decrease from 2001 to 2016. The change in ET was affected by vegetation types. During the study period, the average annual $ET_0$ and AI tended to decrease. At the monthly scale within a year, AI value decreased from January to July and then increased. The interannual variations of $ET_0$ and AI showed periodicity with a main period of 14 a, and two other periodicities of 11 and 5 a. This study showed that in recent years, drought in these pastoral regions of mid-western China has been alleviated. Therefore, it is foreseeable that the demand for irrigation water for agricultural production in these regions will decrease.

**Keywords:** evapotranspiration; aridity index; climate change; human activities; vegetation cover; arid areas

## 1 Introduction

Mid-western China, an arid and semi-arid region, is ecologically important and plays an important role in supporting the livestock husbandry in China. It is one of the most sensitive and fragile areas on the Earth, yet readily influenced by global climate change and human activities. The increase in greenhouse gas concentrations due to human activities has led to surface warming over almost the entire globe (Stocker et al., 2013). Concomitantly, the climate in mid-western China has also been shifting from warm-dry to warm-wet (Shi et al., 2006). Even minor variations in precipitation and temperature can induce significant changes in hydrological processes such as

*Corresponding authors: YANG Huimin (E-mail: huimyang@lzu.edu.cn); FENG Qisheng (E-mail: fengqsh@lzu.edu.cn)
Received 2021-01-23; revised 2021-06-23; accepted 2021-07-23

evapotranspiration (ET) (Gan, 2000; Ma et al., 2004). Additionally, the land surface water cycle and ET are affected by global climate change (Jung et al., 2010; Meng, 2021). Therefore, further documenting the changes in ET and linking them with variations in vegetation cover will contribute to a more comprehensive understanding of agricultural irrigation and ecological water demand, thus promoting the development of agriculture and livestock husbandry.

ET includes the evaporation of water from the Earth's surface and the transpiration of vegetation (Chahine, 1992). It returns about 60.0% of the global terrestrial precipitation to the atmosphere (Wang and Dickinson, 2012) and consumes about 60.0% of the net surface radiation energy (Trenberth et al., 2009). ET links the terrestrial water cycle and surface energy transmission, which determines the intensity of the interactions between the Earth and atmosphere (Jung et al., 2010). In arid areas, global climate change may increase (or decrease) potential evapotranspiration (PET), thereby increasing (or decreasing) the aridity (Huo et al., 2013). Human activities, such as domestic animal husbandry, also play a role in influencing water cycling (Goyal, 2004). In recent years, the potential impact of climate change on reference evapotranspiration ($ET_0$) has been extensively studied (Wang et al., 2019; Liu et al., 2020; Jerin et al., 2021). Long-term climate sequence analysis showed that abrupt climate change occurred in northwestern China around 1975 (Chen et al., 1991). Time series analysis revealed that $ET_0$ decreased in all seasons from 1954 to 1993 in China, especially in northwestern and southeastern areas (Wang et al., 2007; Zhang et al., 2007; Song et al., 2010; Zhang et al., 2010; Thomas, 2015).

Some researchers have analyzed the factors influencing ET changes, revealing that the sensitivity of $ET_0$ changed according to location and associated environmental variables (Liu et al., 2010). For example, Liu et al. (2010) reported that temperature increase was the main cause of $ET_0$ rise in the Yellow River Basin of China. Eslamian et al. (2011) reported that temperature and relative humidity were two most important variables affecting the monthly trend of $ET_0$ in Iran. Espadafor et al. (2011) pointed out that the increases of temperature and solar radiation and the decrease of relative humidity were the main factors leading to the increase of $ET_0$ in southern Spain. Dinpashoh et al. (2011) proved that wind speed was the main cause of $ET_0$ rise in Iran. Li et al. (2013) found that the influence of meteorological factors on $ET_0$ was different in the Heihe River Basin of China at the spatiotemporal scales. Mosaedi et al. (2016) found that sunshine hours, wind speed, and temperature had great effects on $ET_0$ in Iran. Since the late 1980s, some national construction projects and the adjustment of agricultural planting approaches have been implemented in mid-western China, which has affected the environment, including surface vegetation cover. Further exploring ET change and its links with vegetation cover change would be of great help to optimize water management for agriculture production and livestock husbandry in mid-western China.

Ground-based observation can provide data to show time series ET information, but it is difficult to exhibit the spatial distribution characteristics of ET for a broad area when there are not enough observation sites, for instance, in arid mid-western China. By contrast, remote sensing technology can help to obtain the spatial variability of ET at a regional or global scale. Based on the Penman-Monteith equation and moderate-resolution imaging spectroradiometer (MODIS), the global MODIS terrestrial ET (MOD16) data have been released with an accuracy of 86.0% (Mu et al., 2007, 2011). The MOD16 products have been validated and applied in many areas with various climate conditions (Jia et al., 2012; Yang et al., 2014; Chen et al., 2015; Sun et al., 2021). Jia et al. (2012) found that the validation of remotely sensed-ET (RS-ET) at the basin scale showed a good consistency between the 1-km annual RS-ET and the validated data, such as the water balance ET, MODIS ET products, precipitation, and land-use types. Kim et al. (2012) reported that the MOD16 products performed best at five forest sites and were mismatched with observed ET data at two grassland sites in Asia. Feng et al. (2015) pointed out that the MOD16 algorithm reduced the accuracy of ET estimations for grassland, savanna, and shrubland sites over semi-arid ecosystems. In the Tibetan Plateau of China, Chang et al. (2018) also obtained good consistency between the MOD16 products and the measured values. However, the performance of the MOD16 products varies under different climate and underlying surface conditions. Therefore, further investigation on spatiotemporal characteristics of ET using the MOD16 products in

mid-western China would aid understanding of the spatiotemporal distributions and variations of regional ET under global climate change and human activities.

In this study, the MOD16 products were used to analyze the spatiotemporal changes of ET and PET, and ground-based data were used to explore the changes in $ET_0$ and aridity index (AI) in typical mid-western pastoral regions of China, including Gansu Province, Qinghai Province, Ningxia Hui Autonomous Region, and part of Inner Mongolia Autonomous Region. The objectives of this study were to: (1) analyze the spatiotemporal variations of ET and PET; (2) reveal the temporal variations of ET with different vegetation types; and (3) explore the temporal variations of $ET_0$ and AI. It is expected that this study will provide a reference for understanding agricultural irrigation and ecological water demand in mid-western China.

## 2 Materials and methods

### 2.1 Study area

This study was conducted in typical mid-western pastoral regions of China, including Gansu Province, Qinghai Province, Ningxia Hui Autonomous Region, and part of Inner Mongolia Autonomous Region. The longitude range is 89°30′–113°14′E and the latitude range is 33°02′–43°28′N. The elevation is 562–6820 m and the terrain gradually decreases from southwest to northeast. These pastoral regions are characterized by an arid and semi-arid climate with high radiation and heat resources, little precipitation, strong evaporation, and large temperature difference between day and night (Meng et al., 2013; Liu et al., 2021).

### 2.2 MOD16 products

The MODIS ET dataset includes surface ET, latent heat flux, PET, and potential latent heat flux. The dataset has a spatial resolution of 1 km×1 km and time resolutions of 8 d, 1 month, and 1 a. The algorithm is based on the Penman-Monteith equation with some improvements (Mu et al., 2007). These data can better reflect the non-uniformity of the underlying surfaces of desert and oasis, and are suitable for the study of surface ET in arid areas. The annual synthetic product (MOD16) with actual surface ET data was selected, and the time series was from January 2001 to December 2016. The original MODIS products were stored in hierarchical data format (HDF) with sinusoidal projection. HDF files of the MOD16 products were converted into GeoTIFF files using ArcGIS 10.3 and ENVI+IDL (The Environment for Visualizing Images+Interactive Data Language) software. The projection conversion, raster mosaic, resampling, and other operations were performed to organize the final ET data.

### 2.3 Vegetation and meteorological data

The vegetation dataset was provided by the Data Center for Resources and Environmental Sciences, Chinese Academy of Sciences (RESDC) (http://www.resdc.cn). This dataset includes vegetation types, horizontal and vertical distributions, and the relationship of vegetation with climatic factors and surface environmental factors. Distribution of vegetation types in the study area is shown in Figure 1.

The meteorological data (including daily evaporation, precipitation, average temperature, average pressure, relative humidity, and average wind speed) were obtained from 94 meteorological stations (Fig. 1) in the study area from 2001 to 2016. For comparative analysis with ET data, the daily values were processed into 192 monthly and 16 annual values.

### 2.4 Reference evapotranspiration ($ET_0$) and aridity index (AI)

$ET_0$ reflects an important component of the atmosphere-hydrosphere water cycle, which drives the dry-wet conditions on the Earth's surface. The Penman-Monteith equation was recommended by the Food and Agriculture Organization (FAO) for the calculation of $ET_0$ (Allen et al., 2007); it was adopted in this study. The formula below was used to calculate $ET_0$:

$$ET_0 = \frac{0.408\Delta(R_n - G) + 900\gamma / (T + 273)U_2(e_s - e_a)}{\Delta + \gamma(1 + 0.34U_2)}, \quad (1)$$

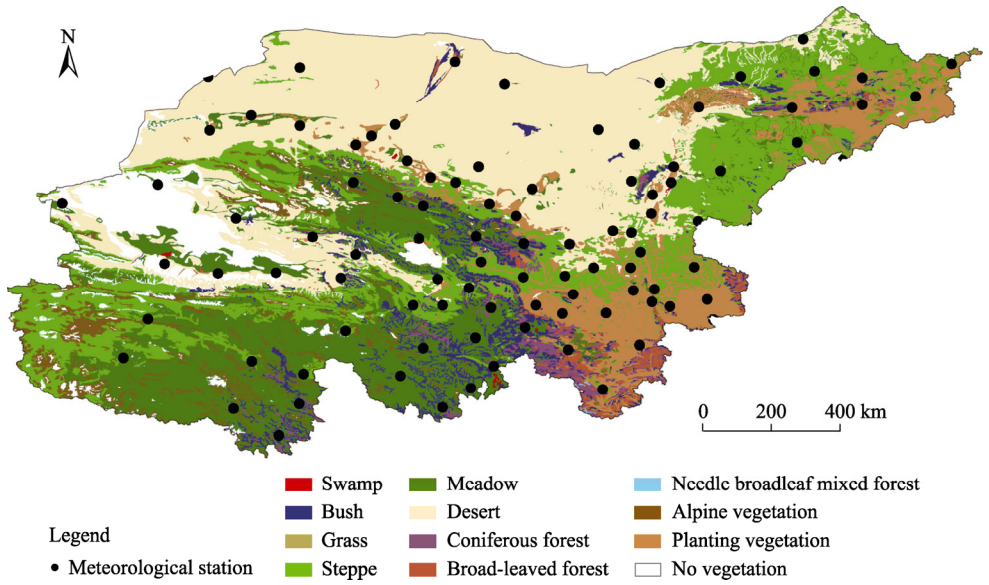


**Fig. 1** Distribution of vegetation types and location of meteorological stations in the study area

where $ET_0$ is the reference evapotranspiration (mm); $R_n$ is the net radiation at the crop surface (MJ/(m$^2$·d)); $G$ is the soil heat flux density (MJ/(m$^2$·d)); $T$ is the mean daily temperature at 2 m height (°C); $U_2$ is the wind speed at 2 m height (m/s); $e_s$ is the saturation vapor pressure (kPa); $e_a$ is the actual vapor pressure (kPa); $\Delta$ is the slope of the vapor pressure curve (kPa/°C); and $\gamma$ is the psychometric constant (kPa/°C).

To further analyze dry-wet conditions in terms of agriculture demand, we also calculated AI. In arid areas, the agricultural aridity is induced mainly by ET exceeding precipitation. $ET_0$ means the reference crop ET determined by climate factors, which can be easily observed (Huo et al., 2013). AI, defined by Thornthwaite (1948), represents the degree of drought in arid or semi-arid areas and is calculated as:

$$\mathrm{AI} = \frac{\mathrm{ET_0} - \mathrm{P}}{\mathrm{ET_0}}, \tag{2}$$

where AI is the aridity index and P is the precipitation (mm). AI can also show the water required to satisfy $ET_0$. If there is no precipitation, AI is equal to 1, and the mean aridity is the highest. By contrast, if precipitation is equal to or higher than $ET_0$, AI is zero or negative. In the study area, as $ET_0$ is greater than precipitation, AI is between 0 and 1.

### 2.5 Interannual variation of evapotranspiration (ET)

The one-way linear regression method (Feng et al., 2015) was used to analyze the temporal variations of annual average ET in the study area with the formula:

$$\theta_{\mathrm{slope}} = \frac{n \times \sum_{j=1}^{n} j \times X_j - \sum_{j=1}^{n} j \sum_{j=1}^{n} X_j}{n \times \sum_{j=1}^{n} j^2 - \left( \sum_{j=1}^{n} j \right)^2}, \tag{3}$$

where $\theta_{\mathrm{slope}}$ is the slope of the trend line; $n$ is the accumulated years of monitoring (a); and $X_j$ is the annual ET of the $j^{\mathrm{th}}$ year (mm). If $\theta_{\mathrm{slope}}>0$, ET increases during the monitored $n$ years, and *vice versa*.

### 2.6 Data analysis

Morlet wavelet analysis has been widely used in many fields, showing the periodic distribution, amplitude, and bit equality information of time series in time domain, and has the ability to

diagnose mutation points in mathematical sense (Ma et al., 2013; Wu et al., 2019; Nourani et al., 2021). Its basic principle is to use a cluster of wavelet function system to represent or approximate a signal or function (Burrus, 2005).

Wavelet function $\Psi(t) \in L^2(R)$ is as follows:

$$\int_{-\infty}^{+\infty} \Psi(t) \mathrm{d}t = 0, \tag{4}$$

where $t$ is time variable (a) and $\Psi(t)$ is a basic wavelet function and can form a cluster of functions:

$$\Psi_{a,b}(t) = |a|^{-\frac{1}{2}} \Psi\left(\frac{t-b}{a}\right), \tag{5}$$

where $\Psi_{a,b}(t)$ is the wavelet transform function; $a$ is the expansion scale; and $b$ is the translation parameter ($a$, $b \in R$, $a \neq 0$).

For $f(t) \in L^2(R)$, the continuous wavelet transform is as follows:

$$\Psi_{a,b}(t) = |a|^{-\frac{1}{2}} \int_R f(t) \overline{\Psi}\left(\frac{t-b}{a}\right) \mathrm{d}t, \tag{6}$$

where $f(t)$ is a signal or square integrable function; $\overline{\Psi}\left(\frac{t-b}{a}\right)$ is a complex conjugate function of $\Psi\left(\frac{t-b}{a}\right)$.

Wavelet variance can be used to determine the relative intensity of different scale disturbances in the signal and the main time scale, i.e., the main period (Burrus, 2005). The formula is as follows:

$$\mathrm{Var}(a) = \int_{-\infty}^{+\infty} |W_f(a, b)|^2 \mathrm{d}b, \tag{7}$$

where $W_f(a, b)$ is wavelet coefficient.

In this study, the wavelet toolkit of MATLAB software was used for wavelet transform. In addition, data processing, analyzing, and drawing were carried out in ArcGIS 10.3, ENVI 5.6, MATLAB 2016, and EXCEL 2010 software.

## 3 Results

### 3.1 Validations of the MOD16 data

The accuracy of the MOD16 data was verified using the correlation coefficient between PET calculated from the MOD16 products and ET observed from the meteorological stations. As shown in Figure 2, at the temporal scale, the correlation coefficient between calculated PET and observed ET was 0.9008 (Fig. 2a) and at the spatial scale, the correlation coefficient between them

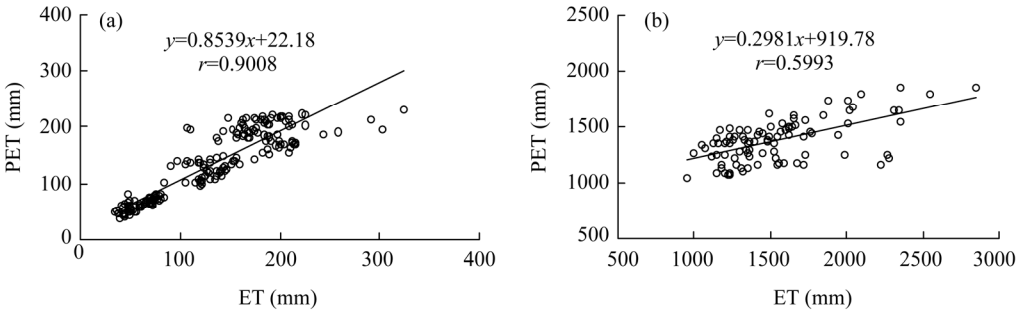


**Fig. 2** Relationships between potential evapotranspiration (PET) calculated from the MOD16 products and evapotranspiration (ET) observed from meteorological stations along a chronosequence (a) and among sites (b) in mid-western China. The data from 192 time points and 94 meteorological stations were used to analyze the relationship between PET calculated from the MOD16 products and ET observed from meteorological stations from 2001 to 2016.

was 0.5993 (Fig. 2b). This showed that PET calculated from the MOD16 products was consistent with ET observed from the meteorological stations, and this dataset from the MOD16 could be used to analyze the spatiotemporal distribution of land surface ET in mid-western China.

### 3.2 Spatiotemporal variations of ET and potential evapotranspiration (PET)

The overall ET in the study area gradually increased from east to southwest (Fig. 3). During the studied 16 a, ET varied from region to region across the study area, but PET was stable.

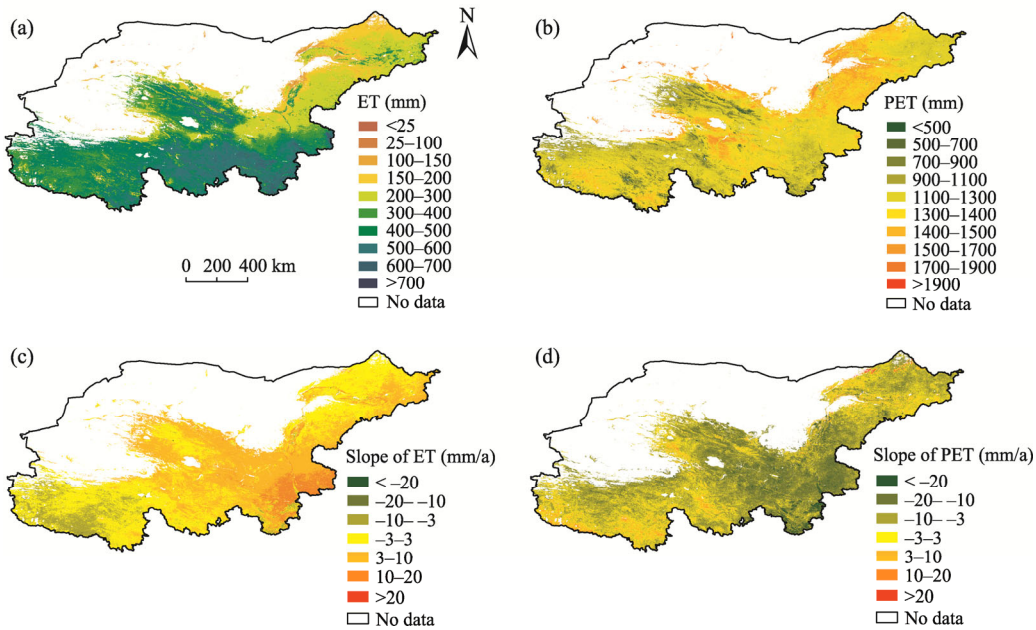


**Fig. 3** Spatial variations of ET (a) and PET (b) as well as spatial variations of slopes of ET (c) and PET (d) in mid-western China. Note that due to the restriction of the MOD16 products, ET in areas without vegetation such as deserts was not calculated and these areas appeared to be blank (white).

From 2001 to 2016, the average annual ET in the study area increased and the difference in magnitude among pastoral regions was obvious, with the order of Qinghai>Gansu>Ningxia> midwestern Inner Mongolia (Fig. 4). The increasing rates of ET were 0.35 mm/a in Qinghai, 8.39 mm/a in Ningxia, 5.90 mm/a in Gansu, and 2.51 mm/a in midwestern Inner Mongolia. The average annual PET, with the range of 980.00–1500.00 mm, showed a decreasing trend during the study period. The order of PET among the four regions was midwestern Inner Mongolia>Ningxia>Gansu>Qinghai. The decreasing rates of PET were 7.00 mm/a in midwestern Inner Mongolia, 11.10 mm/a in Ningxia, 12.00 mm/a in Gansu, and 5.42 mm/a in Qinghai. The difference between PET and ET can explain the water shortage on the land surface, that is, the drought conditions. The differences between PET and ET were large in all four regions, indicating that the overall water condition was dry and water deficit existed. The degree of drought among the four regions was in the order of midwestern Inner Mongolia>Ningxia>Gansu>Qinghai. The trends of PET were decreasing, showing that drought conditions in different regions were mitigated.

### 3.3 Average monthly ET and PET changes

The trend of average monthly ET and PET changes in various pastoral regions was dominated by the higher ET in summer and the lower ET in other seasons, and both ET and PET tended to increase first and then decrease at the monthly scale (Fig. 5). The maximum monthly ET in Gansu, midwestern Inner Mongolia, Ningxia, and Qinghai was 61.85, 27.50, 36.20, and 61.10 mm, respectively. The minimum monthly ET in Gansu, midwestern Inner Mongolia, Ningxia, and Qinghai was 24.63, 10.79, 16.17, and 26.32 mm, respectively, which respectively occurred in December, May, April, and December. The minimum monthly PET in the study area was in

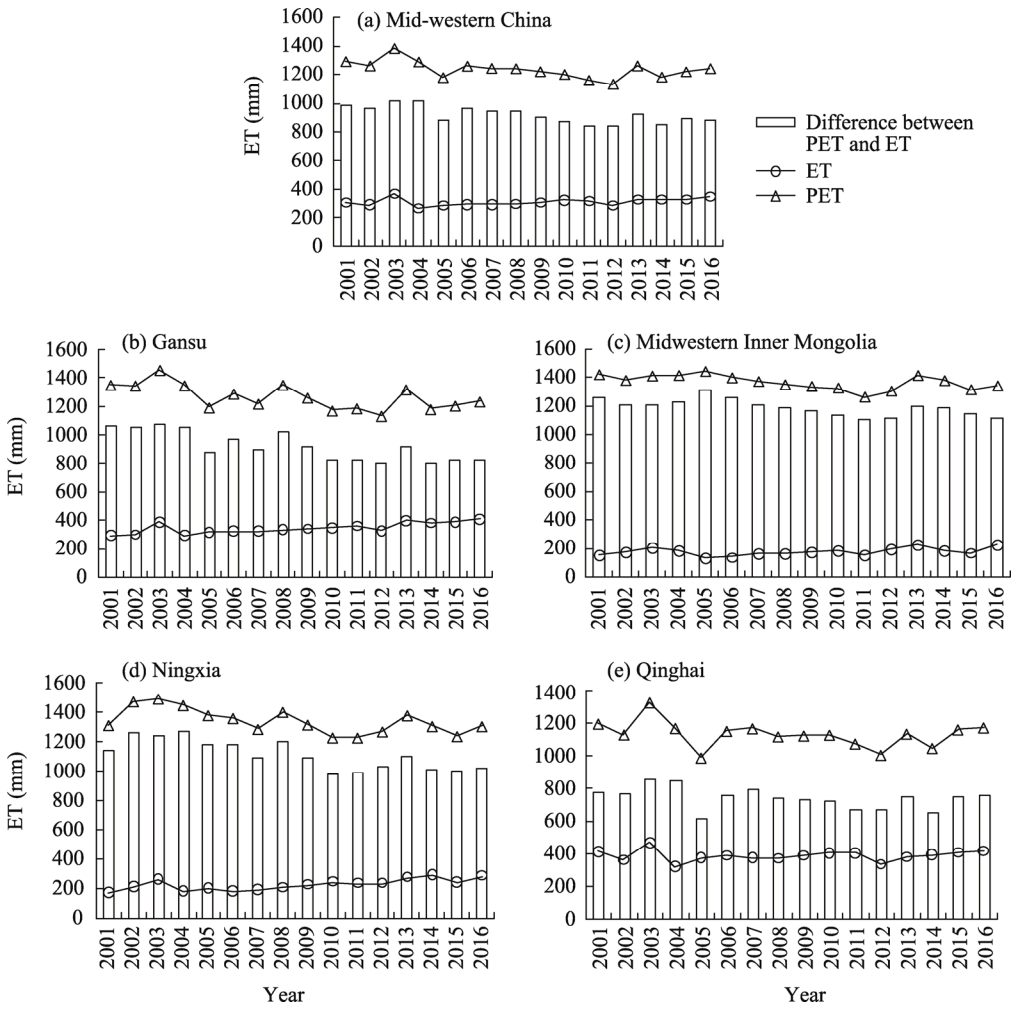


**Fig. 4** Average annual variations of ET and PET in mid-western China (a) as well as in the pastoral regions of Gansu (b), midwestern Inner Mongolia (c), Ningxia (d), and Qinghai (e) during 2001–2016

December, with the values of 51.31, 34.35, 45.03, and 43.60 mm in Gansu, midwestern Inner Mongolia, Ningxia, and Qinghai, respectively. The maximum monthly PET was 209.03 mm in Gansu, 229.10 mm in midwestern Inner Mongolia, 219.27 mm in Ningxia, and 190.85 mm in Qinghai. The maximum difference between the average monthly PET and the average monthly ET in Gansu and midwestern Inner Mongolia was 153.90 and 207.80 mm in May, respectively, whereas it was 190.53 mm in June for Ningxia and 129.75 mm in July for Qinghai.

### 3.4 Interannual variations and monthly changes of ET in different vegetation types

From 2001 to 2016, the interannual variation of ET for each vegetation type showed a steadily increasing trend (Fig. 6). The average annual ET over the study period in different vegetation types was as followed: forest (386.85 mm), shrub (337.68 mm), alpine vegetation (303.77 mm), natural grassland (296.50 mm), cultivated vegetation (286.39 mm), swamp (279.19 mm), and desert (187.72 mm).

The change of monthly ET was significantly different in different vegetation types (Fig. 6). The trend can be roughly divided into three categories. First, there was a single peak mainly for forest; specifically, monthly ET increased from January and decreased after reaching the maximum in July at the monthly scale. Second, monthly ET fluctuated in natural grassland, desert, cultivated vegetation, and swamp; specifically, monthly ET firstly decreased from January to April and then increased to peak in July and/or August. After reaching the peak value, monthly ET decreased and

later increased again. Third, monthly ET exhibited a bimodal type for alpine vegetation and shrubs. For this category, monthly ET first slowly increased till March, slightly decreased in April, then rapidly increased to peak in July, and finally decreased.

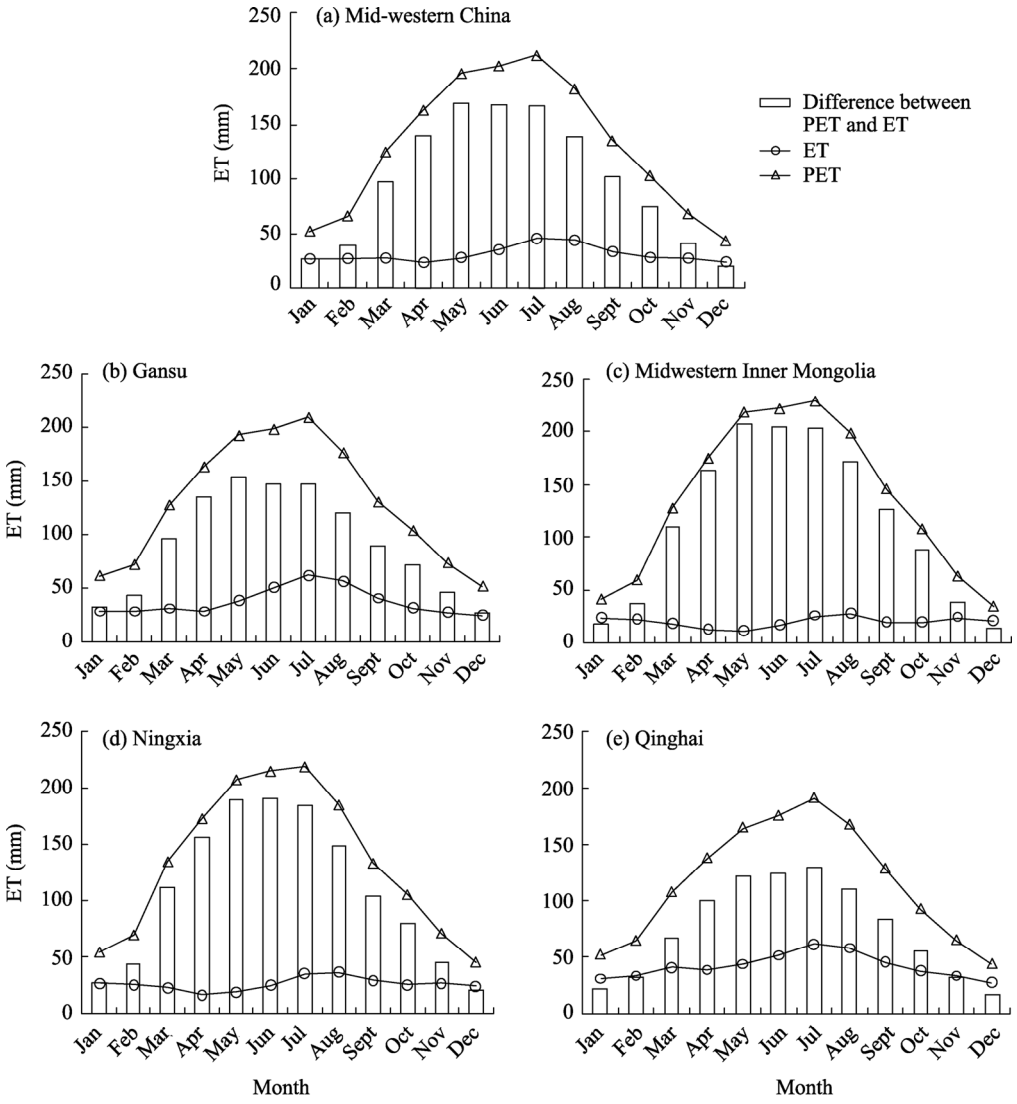


**Fig. 5** Average monthly ET and PET changes in mid-western China (a) as well as in the pastoral regions of Gansu (b), midwestern Inner Mongolia (c), Ningxia (d), and Qinghai (e) during 2001–2016

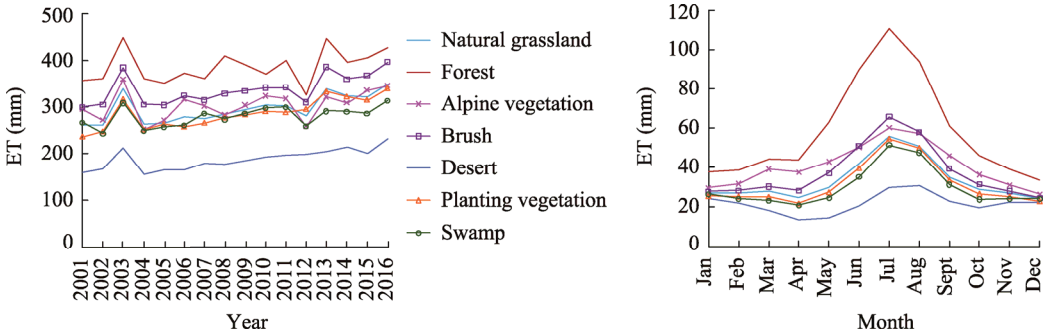


**Fig. 6** Interannual variations (a) and monthly changes (b) of ET in different vegetation types in mid-western China

### 3.5 Interannual variations and monthly changes of $ET_0$, AI, and precipitation

Linear regression analysis showed that the average annual $ET_0$ and AI in the study area decreased from 2001 to 2016 (Fig. 7). Specifically, the average annual $ET_0$ demonstrated a significant decline trend at a rate of 12.90 mm/a, and the average annual AI decreased by 0.03 mm/decade. By contrast, the average annual precipitation increased from 2001 to 2016, at a rate of 1.98 mm/a. It should be noted that the changes of average annual AI and the average annual precipitation were not statistically significant.

The average monthly $ET_0$, precipitation, and AI had significant seasonal variations (Fig. 7b). Overall, both $ET_0$ and precipitation increased first and then decreased at the monthly scale, while AI exhibited the opposite trend and was greater than 0.60. This indicated that the study area belonged to an arid area and the climate was dry throughout the year. In July, $ET_0$ reached the maximum with a value of 183.94 mm, and precipitation also had the maximum value in July with a value of 63.34 mm. Both the temporal trends of $ET_0$ and precipitation caused a minimum AI of 0.60 in July. During the periods of January–April and November–December, AI was higher than 0.90.

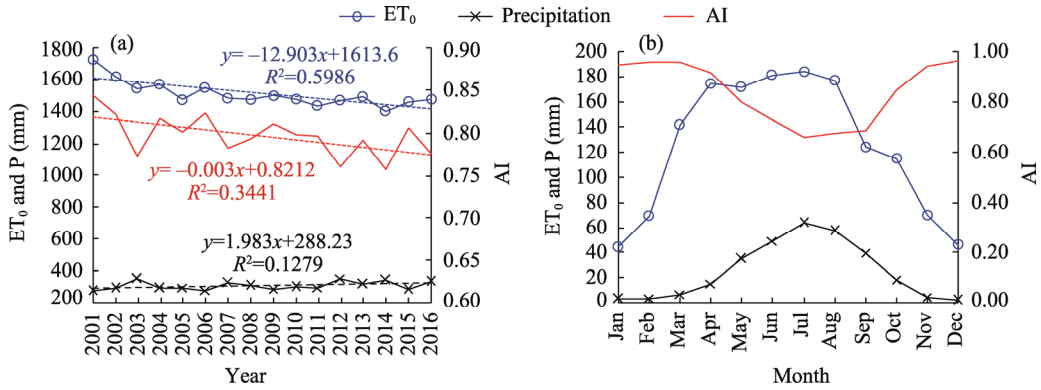


**Fig. 7** Interannual variations (a) and monthly changes (b) of average reference evapotranspiration ($ET_0$), precipitation, and arid index (AI) in mid-western China

### 3.6 Periodic features of $ET_0$ and AI

Morlet wavelet analysis revealed that $ET_0$ and AI had obvious localization characteristics at the interannual time scale, with nested signal strength and phase, and uneven frequency and time domain distribution (Fig. 8). The variation of annual $ET_0$ had a long periodicity of 10–16 a, and there was also a short periodicity of 4–6 a. Therefore, annual $ET_0$ had three periodicities: 5, 11, and 14 a, indicating that the change of annual $ET_0$ had a major periodicity of 14 a, a secondary periodicity of 11 a, and a minor periodicity of 5 a. The major and secondary periodicities of annual AI were consistent with those of annual $ET_0$, but annual AI still had shorter periodicities of about 3 and 6 a.

## 4 Discussion

### 4.1 Applicability of the MOD16 products in arid and semi-arid areas

In recent years, the MOD16 products are widely used in hydrological research in arid and semi-arid areas where ground-based data are scarce (Khan et al., 2018; Li et al., 2021; Wang et al., 2021). For example, Glenn et al. (2011) used the MOD16 products to capture the general actual ET as well as its features and trends at a continental scale in Australia. Mu et al. (2011) compared the MOD16 derived ET data with measured ET data from 46 AmeriFlux eddy covariance flux towers located across seven biomes in North America and found that the average error was 24.1%, within the accuracy range of multiple remote sensing methods (10.0%–30.0%) (Kalma et al., 2008). Moreira et al. (2018) evaluated the performance of the MOD16 products in nine eddy covariance monitoring sites from the Large-Scale Biosphere-Atmosphere Experiment in the Amazon and revealed that the products showed similar ET values with the calculated

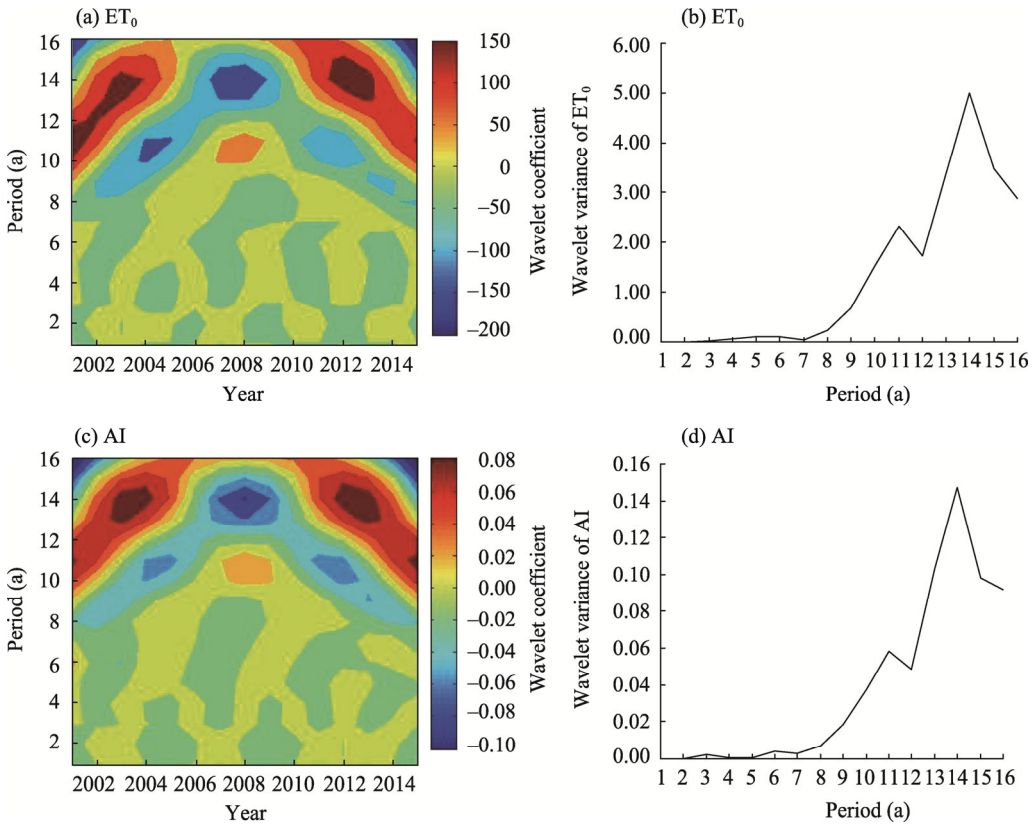


**Fig. 8** Morlet wavelet analysis of periodic features of average $ET_0$ (a, b) and AI (c, d) in mid-western China

statistics. Although the accuracy of the MOD16 products still needs to be further verified in semi-arid areas, it is helpful to identify the spatiotemporal trends of ET change (Jovanovic et al., 2015). Concerns have also arisen on the short duration of the MOD16 dataset (only from the last 20 a). Therefore, it is better to use additional datasets from the MOD16 products over a longer duration to demonstrate ET change associated with climate change.

### 4.2 Effects of vegetation type and climate change on ET

In this study, actual ET in mid-western China increased year to year, although the trend was not significant. This is because the amount of ET is closely related to both vegetation type and climate change. Vegetation connects the soil to the atmosphere and regulates water balance, so higher vegetation cover can facilitate water cycling. In recent years, global warming and significant increase in vegetation cover in Northwest China (Mou et al., 2018) have led to an increase in ET. Mo et al. (2014) showed that NDVI (Normalized Difference Vegetation Index) was positively correlated with ET in China. We also found PET exhibited a slightly decreasing trend with years in mid-western China, which is consistent with the finding in Northwest China revealed by Yang et al. (2015). The declining trend of PET suggested that drought stress was ameliorated (Yao et al., 2015). Precipitation in Northwest China was gradually increasing in recent years (Chen et al., 2014), and there was a significant negative relationship between precipitation and PET (Pan et al., 2021). Additionally, the variation of PET was possibly affected by other atmospheric factors, such as solar radiation, wind speed, and temperature (Baguis et al., 2010; Thomas, 2015; Feng et al., 2019).

In this study, ET in mid-western China changed in an obvious season-specific way. There was little precipitation from January to April in this area and surface water could not be replenished, which results in a decreasing tendency of ET. In April, vegetative plants began to grow, leading to an increase of ET. In the northwest pastoral areas, the land use/cover types were complex, including desert, wind- and sand-controlled engineering areas, and the forests and grasslands

were converted from farmlands. These areas tended to have a low vegetation cover and the existing vegetation was mainly cultivated vegetation that can absorb shallow soil moisture. Therefore, the increase of ET was not significant. In July and August, precipitation was concentrated, thus ET reached the highest value. Moreover, solar radiation was a major factor affecting ET (He et al., 2015). Summer days were long, receiving the most solar radiation and promoting the growth of natural and cultivated vegetation. Surface water circulation was accelerated from June to August, and ET continued to increase. In this study, the seasonal response of ET varied in different pastoral regions. The lowest ET in mid-western Inner Mongolia and Ningxia occurred in May and April, respectively, and ET in Gansu was also at a minimum value in April. This is probably because of the snow melting in spring and the gradually increased temperature. Appropriate temperature and moisture were beneficial for grass or crop re-greening, and ET in this period was lower than that in other times of the year (Tong et al., 2016).

The ET of all individual vegetation types changed similarly to the overall ET in mid-western China. However, vegetation types varied in different pastoral regions of the study area and land use/cover types were diversified, resulting in at least three types of monthly ET change trends. We found there was a decrease in ET around April for some vegetation types. In spring, natural vegetation began to regrow, but grazing and human activities (such as plowing) would lead to a reduction of vegetation cover. Considering low precipitation in this season, the decrease in ET can be predicted. After spring, temperature and precipitation gradually increased, providing adequate heat and water for the rapid growth of vegetation, which leads to a rapid rise of ET to peak around August.

### 4.3 Periodic changes of AI and $ET_0$

The variation of $ET_0$ was influenced by radiometric and aerodynamic variables, which mainly reflect the changes in topography and climate (McVicar et al., 2007; Huo et al., 2013; Collins et al., 2021). In this study, $ET_0$ fluctuated and decreased during the studied 16-a duration. This was consistent with the studies conducted in India (Chattopadhyay and Hulme, 1997), and the Yangtze River Basin (Xu et al., 2006) and the Yellow River Basin in China (Zhang et al., 2015). The decreasing trend of $ET_0$ was mainly attributed to the decreases in net total radiation and wind speed (Zhang et al., 2015). However, Tabari (2010) showed that average annual $ET_0$ increased by 2.30–11.30 mm in an arid western area of Iran, which may be related to the higher temperature. Nouri and Bannayan (2019) suggested that the variation trend of $ET_0$ was regulated by mean temperature and wind speed in humid environment.

In this study, we also found that AI decreased in mid-western China, suggesting the whole area became wetter. This was consistent with previous results (Wang et al., 2007; Liu et al., 2013). Vegetation cover has increased in this study area during the period from 2001 to 2015 (Mou et al., 2018) and there was a humidification trend in Northwest China based on the study of a dry-wet homogenization index (Wang et al., 2007). Analysis of the monthly changes of $ET_0$ and AI showed that there was a unimodal change for $ET_0$ and an opposite change for AI within a year in this study. Past studies revealed that temperature played a decisive role in regulating water cycle in most arid areas, such as Iran (Bazrafshan, 2017). AI was significantly and negatively correlated with precipitation, which contributed 91.7% of the decrease in AI in Northwest China from 1960 to 2010 (Liu et al., 2013). In this study, temperature and precipitation in mid-western China were higher from June to August, leading to the greatest $ET_0$; during this period, AI was the lowest, indicating the wettest time of the year. Zhang et al. (2015) found that the periodic periods of $ET_0$ and AI were 4–6, 8–12, and 18–22 a in the Yellow River Basin, China. The periodicity of $ET_0$ was similar to that of AI to some extent, and the major periodicities of the two variables were comparable. Also, the periodic changes of AI and $ET_0$ were affected by macroclimate patterns, such as El Niño, and atmospheric circulation (Zhang et al., 2015). Atmospheric circulation had a periodicity of 2–4 a, and it took 2–7 a for each El Niño to occur (Fan, 2018). However, the relationship of periodic changes of AI and $ET_0$ with global warming still needs to be explored with long-time monitoring.

## 5 Conclusions

The overall ET gradually increased from east to southwest in mid-western China. From 2001 to 2016, actual ET showed an increasing trend, whereas PET decreased. The average annual ET variation in different vegetation types can be divided into unimodal, fluctuation, and bimodal patterns. The average annual $ET_0$ and AI decreased during the studied 16-a duration. The interannual variations of $ET_0$ and AI showed obvious periodic changes with a major periodicity of 14 a, a secondary periodicity of 11 a, and a minor periodicity of about 5 a. This study showed that drought has been alleviated in mid-western pastoral regions of China in recent years. Therefore, a decrease in irrigation water demand may be foreseen for agricultural production. This research will help clarify irrigational and ecological water requirements and guide irrigation management for the development of agriculture and animal husbandry in arid areas.

## Acknowledgements

This work was supported by the earmarked fund for China Agriculture Research System of Ministry of Finance and Ministry of Agriculture and Rural Affairs (CARS-34) and the National Key Research and Development Program of China (2016YFC0400302).



### References

Allen R G, Tasumi M, Morse A, et al. 2007. Satellite-based energy balance for mapping evapotranspiration with internalized calibration (METRIC)—Applications. Journal of Irrigation and Drainage Engineering, 133(4): 380–394.

Baguis P, Roulin E, Willems P, et al. 2010. Climate change scenarios for precipitation and potential evapotranspiration over central Belgium. Theoretical and Applied Climatology, 99(3–4): 273–286.

Bazrafshan J. 2017. Effect of air temperature on historical trend of long-term droughts in different climates of Iran. Water Resources Management, 31: 4683–4698.

Burrus C S. 2005. Introduction to Wavelets and Wavelet Transforms: A Primer. Beijing: China Machine Press.

Chahine M T. 1992. The hydrological cycle and its influence on climate. Nature, 359: 373–380.

Chang Y P, Qin D H, Ding Y J, et al. 2018. A modified MOD16 algorithm to estimate evapotranspiration over alpine meadow on the Tibetan Plateau, China. Journal of Hydrology, 561: 16–30.

Chattopadhyay N, Hulme M. 1997. Evaporation and potential evapotranspiration in India under conditions of recent and future climate change. Agricultural and Forest Meteorology, 87(1): 55–73.

Chen L X, Shao Y N, Zhang Q F, et al. 1991. Preliminary analysis of climatic change during the last 39 years in China. Quarterly Journal of Applied Meteorology, 2(2): 164–169. (in Chinese)

Chen R, Liu J, Kang E, et al. 2015. Precipitation measurement intercomparison in the Qilian Mountains, north-eastern Tibetan Plateau. The Cryosphere Discussions, 9(5): 1995–2008.

Chen Y N, Li Z, Fan Y T, et al. 2014. Research progress on the impact of climate change on water resources in the arid region of Northwest China. Acta Geographica Sinica, 69(9): 1295–1304. (in Chinese)

Collins B, Ramezani Etedali H, Tavakol A, et al. 2021. Spatiotemporal variations of evapotranspiration and reference crop water requirement over 1957–2016 in Iran based on CRU TS gridded dataset. Journal of Arid Land, 13(8): 858–878.

Dinpashoh Y, Jhajharia D, Fakheri-Fard A, et al. 2011. Trends in reference crop evapotranspiration over Iran. Journal of Hydrology, 399(3–4): 422–433.

Eslamian S, Khordadi M J, Abedi-Koupai J. 2011. Effects of variations in climatic parameters on evapotranspiration in the arid and semi-arid regions. Global and Planetary Change, 78(3–4): 188–194.

Espadafor M, Lorite I J, Gavilán P, et al. 2011. An analysis of the tendency of reference evapotranspiration estimates and other climate variables during the last 45 years in southern Spain. Agricultural Water Management, 98(6): 1045–1061.

Fan S P. 2018. Variation tendency of potential evapotranspiration and aridity index in Central Gansu Province in recent 55 years. Journal of Earth Environment, 9(2): 172–181. (in Chinese)

Feng F, Chen J Q, Li X L, et al. 2015. Validity of five satellite-based latent heat flux algorithms for semi-arid ecosystems. Remote Sensing, 7(12): 16733–16755.

Feng X, Thompson S E, Woods R, et al. 2019. Quantifying asynchronicity of precipitation and potential evapotranspiration in Mediterranean climates. Geophysical Research Letters, 46(24): 14692–14701.

Gan T Y. 2000. Reducing vulnerability of water resources of Canadian Prairies to potential droughts and possible climatic warming. Water Resources Management, 14(2): 111–135.

Glenn E P, Doody T M, Guerschman J P, et al. 2011. Actual evapotranspiration estimation by ground and remote sensing methods: the Australian experience. Hydrological Processes, 25(26): 4103–4116.

Goyal R K. 2004. Sensitivity of evapotranspiration to global warming: A case study of arid zone of Rajasthan (India). Agricultural Water Management, 69(1): 1–11.

He H J, Zhuo J, Dong J F, et al. 2015. Surveying variations of evapotranspiration in Shaanxi Province using MOD16 products. Arid Land Geography, 38(5): 960–967. (in Chinese)

Huo Z L, Dai X Q, Feng S Y, et al. 2013. Effect of climate change on reference evapotranspiration and aridity index in arid region of China. Journal of Hydrology, 492(7): 24–34.

Jerin J N, Islam H M T, Islam A R M T, et al. 2021. Spatiotemporal trends in reference evapotranspiration and its driving factors in Bangladesh. Theoretical and Applied Climatology, 144: 793–808.

Jia Z Z, Liu S M, Xu Z W, et al. 2012. Validation of remotely sensed evapotranspiration over the Hai River Basin, China. Journal of Geophysical Research, 117, doi: 10.1029/2011JD017037.

Jovanovic N, Mu Q S, Bugan R D H, et al. 2015. Dynamics of MODIS evapotranspiration in South Africa. Water SA, 41(1): 79–90.

Jung M, Reichstein M, Ciais P, et al. 2010. Recent decline in the global land evapotranspiration trend due to limited moisture supply. Nature, 467(7318): 951–954.

Kalma J D, McVicar T R, McCabe M F. 2008. Estimating land surface evaporation: a review of methods using remotely sensed surface temperature data. Surveys in Geophysics, 29: 421–469.

Khan M S, Liaqat U W, Baik J, et al. 2018. Stand-alone uncertainty characterization of GLEAM, GLDAS and MOD16 evapotranspiration products using an extended triple collocation approach. Agricultural and Forest Meteorology, 252(15): 256–268.

Kim H W, Hwang K, Mu Q Z, et al. 2012. Validation of MODIS 16 global terrestrial evapotranspiration products in various climates and land cover types in Asia. KSCE Journal of Civil Engineering, 16(2): 229–238.

Li M, Chu R, Islam A, et al. 2021. Characteristics of surface evapotranspiration and its response to climate and land use and land cover in the Huai River Basin of eastern China. Environmental Science and Pollution Research, 28(1): 683–699.

Li Z L, Li Z J, Xu Z X, et al. 2013. Temporal variations of reference evapotranspiration in Heihe River basin of China. Hydrology Research, 44(5): 904–916.

Liu M G, Wang Z K, Mu L, et al. 2021. Effect of regulated deficit irrigation on alfalfa performance under two irrigation systems in the inland arid area of midwestern China. Agricultural Water Management, 248: 106764, doi: org/10.1016/j.agwat.2021.106764.

Liu Q, Yang Z F, Cui B S, et al. 2010. The temporal trends of reference evapotranspiration and its sensitivity to key meteorological variables in the Yellow River Basin, China. Hydrological Processes, 24(15): 2171–2181.

Liu X M, Zhang D, Luo Y Z, et al. 2013. Spatial and temporal changes in aridity index in northwest China: 1960 to 2010. Theoretical and Applied Climatology, 112: 307–316.

Liu Y, Wang Q Y, Yao X L, et al. 2020. Variation in reference evapotranspiration over the Tibetan Plateau during 1961–2017: Spatiotemporal variations, future trends and links to other climatic factors. Water, 12: 3178, doi: 10.3390/w12113178.

Ma J Z, Chen L H, He J H, et al. 2013. Trends and periodicities in observed temperature, precipitation and runoff in a desert catchment: case study for the Shiyang River Basin in Northwestern China. Water and Environment Journal, 27(1): 86–98.

Ma Z G, Dan L, Hu Y W. 2004. The extreme dry/wet events in northern China during recent 100 years. Journal of Geographical Sciences, 14(3): 275–281.

McVicar T R, Niel T G V, Li L T, et al. 2007. Spatially distributing monthly reference evapotranspiration and pan evaporation considering topographic influences. Journal of Hydrology, 338(3–4): 196–220.

Meng C L. 2021. Water balance scheme development for urban modelling. Urban Climate, 37(9): 100843, doi: 10.1016/j.uclim.2021.100843.

Meng X J, Zhang S F, Zhang Y Y, et al. 2013. Temporal and spatial changes of temperature and precipitation in Hexi Corridor during 1955–2011. Journal of Geographical Sciences, 23(4): 653–667. (in Chinese)

Mo X, Liu S, Lin Z, et al. 2014. Trends in land surface evapotranspiration across China with remotely sensed NDVI and climatological data for 1981–2010. Hydrological Sciences Journal, 60(12): 2163–2177.

Moreira A A, Adamatti D S, Ruhoff A L. 2018. Evaluation of remotely sensed evapotranspiration products MOD16 and GLEAM in eddy covariance flux sites from LBA Project. Micrometeorologia, 40: 112–118.

Mosaedi A, Sough M G, Sadeghi S H, et al. 2016. Sensitivity analysis of monthly reference crop evapotranspiration trends in Iran: a qualitative approach. Theoretical and Applied Climatology, 128(3–4): 857–873.

Mou L, Lu Y X, Yang H M, et al. 2018. Spatiotemporal variation of vegetation cover in the pastoral area in Northwestern China during the period of 1981–2015. Arid Zone Research, 35(3): 615–623. (in Chinese)

Mu Q Z, Heinsch F A, Zhao M S, et al. 2007. Development of a global evapotranspiration algorithm based on MODIS and global meteorology data. Remote Sensing of Environment, 111(4): 519–536.

Mu Q Z, Zhao M S, Running S W. 2011. Improvements to a MODIS global terrestrial evapotranspiration algorithm. Remote Sensing of Environment, 115(8): 1781–1800.

Nourani V, Tootoonchi R, Andaryani S. 2021. Investigation of climate, land cover and lake level pattern changes and interactions using remotely sensed data and wavelet analysis. Ecological Informatics, 64: 101330, doi: 10.1016/j.ecoinf.2021.101330.

Nouri M, Bannayan M. 2019. Spatiotemporal changes in aridity index and reference evapotranspiration over semi-arid and humid regions of Iran: Trend, cause, and sensitivity analyses. Theoretical and applied climatology, 136(3–4): 1073–1084.

Pan N, Wang S, Liu Y X, et al. 2021. Rapid increase of potential evapotranspiration weakens the effect of precipitation on aridity in global drylands. Journal of Arid Environments, 186: 104414, doi: 10.1016/j.jaridenv.2020.104414.

Shi Y F, Shen Y P, Kang E, et al. 2006. Recent and future climate change in northwest China. Climatic Change, 80(3–4): 379–393.

Song Z W, Zhang H L, Snyder R L, et al. 2010. Distribution and trends in reference evapotranspiration in the north China plain. Journal of Irrigation and Drainage Engineering, 136(4): 240–247.

Stocker T F, Qin D, Plattner G K, et al. 2013. IPCC, 2013: Summary for Policymakers. In: Climate Change 2013: The Physical Science Basis. Contribution of Working Group I to the Fifth Assessment Report of the Intergovernmental Panel on Climate Change. Cambridge and New York: Cambridge University Press.

Sun Z D, Lotz T, Huang Q. 2021. An ET-based two-phase method for the calibration and application of distributed hydrological models. Water Resources Management, 35(3): 1065–1077.

Tabari H. 2010. Evaluation of reference crop evapotranspiration equations in various climates. Water Resources Management, 24(10): 2311–2337.

Thomas A. 2015. Spatial and temporal characteristics of potential evapotranspiration trends over China. International Journal of Climatology, 20(4): 381–396.

Thornthwaite C W. 1948. An approach toward a rational classification of climate. Geographical Review, 38(1): 55–89.

Tong S Q, Zhang J Q, Hasi, et al. 2016. 14 years spatial-temporal distribution characteristics of evapotranspiration in Xilingol grassland based on MOD16. Chinese Journal of Grassland, 38(4): 83–91. (in Chinese)

Trenberth K E, Fasullo J T, Kiehl J. 2009. Earth's global energy budget. Bulletin of the American Meteorological Society, 90(3): 311–324.

Wang K C, Dickinson R E. 2012. A review of global terrestrial evapotranspiration: Observation, modeling, climatology, and climatic variability. Reviews of Geophysics, 50(2): 1–54.

Wang P X, Zheng Y F, He J H, et al. 2007. Analysis of climate change from dry to wet phase in NW China with an aridity-wetness homogenized index. In: IEEE International Geoscience and Remote Sensing Symposium, IGARSS 2007. Barcelona: 1778–1781, doi: 10.1109/IGARSS.2007.4423165.

Wang S, Lian J J, Peng Y Z, et al. 2019. Generalized reference evapotranspiration models with limited climatic data based on random forest and gene expression programming in Guangxi, China. Agricultural Water Management, 221: 220–230.

Wang Y, Jiang T, Bothe O, et al. 2007. Changes of pan evaporation and reference evapotranspiration in the Yangtze River basin. Theoretical and Applied Climatology, 90: 13–23.

Wang Y P, Li R, Hu J H, et al. 2021. Evaluations of MODIS and microwave based satellite evapotranspiration products under varied cloud conditions over East Asia forests. Remote Sensing of Environment, 264(5): 112606, doi: 10.1016/j.rse.2021.112606.

Wu S Q, Cao S S, Wang Z H, et al. 2019. Spatiotemporal variations in agricultural flooding in middle and lower reaches of Yangtze River from 1970 to 2018. Sustainability, 11(23): 6613.

Xu C Y, Gong L B, Jiang T, et al. 2006. Analysis of spatial distribution and temporal trend of reference evapotranspiration and pan evaporation in Changjiang (Yangtze River) catchment. Journal of Hydrology, 327(1–2): 81–93.

Yang C, Xia J Z, Liang S L, et al. 2014. Comparison of satellite-based evapotranspiration models over terrestrial ecosystems in China. Remote Sensing of Environment, 140: 279–293.

Yang X Q, Wang G J, Pan X, et al. 2015. Spatio-temporal variability of terrestrial evapotranspiration in China from 1980 to 2011 based on GLEAM data. Transactions of the Chinese Society of Agricultural Engineering, 31(21): 132–141. (in Chinese)

Yao J Q, Yang Q, Liu Z H, et al. 2015. Spatio-temporal change of precipitation in arid region of the northwest China. Acta Ecologica Sinica, 35(17): 5846–5855. (in Chinese)

Zhang K X, Pan S M, Zhang W, et al. 2015. Influence of climate change on reference evapotranspiration and aridity index and their temporal-spatial variations in the Yellow River Basin, China, from 1961 to 2012. Quaternary International, 380–381: 75–82.

Zhang S H, Wang Y F, Hou Q Z, et al. 2015. Spatial and temporal characteristics of aridity index and association with AO and ENSO in Qinghai Province. Pratacultural Science, 32(12): 1980–1987. (in Chinese)

Zhang X T, Kang S Z, Zhang L, et al. 2010. Spatial variation of climatology monthly crop reference evapotranspiration and sensitivity coefficients in Shiyang river basin of northwest China. Agricultural Water Management, 97(10): 1506–1516.

Zhang Y Q, Liu C M, Tang Y H, et al. 2007. Trends in pan evaporation and reference and actual evapotranspiration across the Tibetan Plateau. Journal of Geophysical Research, 112, doi: 10.1029/2006jd008161.